Fabrication of 40 Gb/s Front-End Optical Receivers Using Spot-Size Converter Integrated Waveguide Photodiodes

Yong-Hwan Kwon, Joong-Seon Choe, Jeha Kim, Kisoo Kim, Kwang-Seong Choi, Byung-Seok Choi, and HoGyeong Yun

We fabricated 40 Gb/s front-end optical receivers using spot-size converter integrated waveguide photodiodes (SSC-WGPDs). The fabricated SSC-WGPD chips showed a high responsivity of approximately 0.8 A/W and a 3 dB bandwidth of approximately 40 GHz. A selective wet-etching method was first adopted to realize the required width and depth of a tapered waveguide. Two types of electrical pre-amplifier chips were used in our study. One has higher gain and the other has a broader bandwidth. The 3 dB bandwidths of the higher gain and broader bandwidth modules were about 32 and 42 GHz, respectively. Clear 40 Gb/s non-return-to-zero (NRZ) eye diagrams showed good system applicability of these modules.

Keywords: Waveguide photodiode, spot-size converter, optical receiver, selective wet-etching.

I. Introduction

The world's first ultra-long-haul optical transmission field trial at 40 Gb/s on a 1200 km link was demonstrated between Sacramento and Salt Lake City in June 2004 by MCI, Inc. [1]. Although the upper limit of the single-channel transmission unit capacity of a SONET/SDH (synchronous optical network/synchronous digital hierarchy) system is 10 Gb/s at present, a 40 Gb/s transmission technology is believed to be a strong candidate for next-generation Tbps communication networks. Therefore, it is crucial to secure state-of-the-art 40 Gb/s optical components at low cost. Among these, 40 Gb/s front-end optical receivers consisting of photodiodes (PDs) and electrical pre-amplifiers are essential components for determining the sensitivity of all the receiving parts [2].

While side-illuminated waveguide PDs (WGPDs) are superior to vertically-illuminated PDs in intrinsic responsivity level for 40 Gb/s applications due to their increased absorption volume [3]-[7], it is practically difficult to achieve high responsivity due to a large mode-size mismatch between a WGPD (<1 μm) and single-mode optical fiber (about 10 μm). Therefore, there have been studies on optimizing the mode-size of a WGPD and optical coupling [5]-[7]. Among these, a spot-size-converter (SSC) technology was employed in this study to enable high coupling efficiency and to improve the responsivity of WGPDs and thus the sensitivity of receivers.

In this study, we fabricated 40 Gb/s front-end optical receivers using SSC-integrated WGPDs (SSC-WGPDs). A selective wet-etching method and its compatible device structures were

Manuscript received Jan. 24, 2005; revised May 19, 2005.

The material in this work was presented in part at IT-SoC 2004, Seoul, Korea, Oct. 2004.

Yong-Hwan Kwon (phone: +82 42 860 5377, email: yhkwon@etri.re.kr), Joong-Seon Choe (email: jschoe@etri.re.kr), Jeha Kim (email: jeha@etri.re.kr), Kisoo Kim (email: kimks1136@etri.re.kr), Kwang-Seong Choi (email: kwchoi@etri.re.kr), Byung-Seok Choi (email: chbs@etri.re.kr), and HoGyeong Yun (email: yunhg@etri.re.kr) are with Basic Research Laboratory, ETRI, Daejeon, Korea.

suggested to realize the laterally tapered SSC waveguides, which helps to improve the reproducibility of the SSC fabrication process. Two types of commercial transimpedance amplifiers (TIAs) from Inphi, Inc., were used as electrical pre-amplifiers [8], [9]. One amplifier (4331TA) has higher gain and the other (4335TA) has broader bandwidth. The 3 dB bandwidths of higher gain and broader bandwidth modules were measured to be around 32 and 42 GHz, respectively. High speed packaging technologies based on High-Frequency Structure Simulator (HFSS) simulation were developed to secure the high-frequency characteristics of front-end receiver modules. The 40 Gb/s non-return-to-zero (NRZ) eye diagrams for these modules showed clear eyes and indicated perfect applicability of these modules to 40 Gb/s communication systems.

II. Fabrication of SSC-WGPD

A schematic diagram and microscopic image of an SSC-WGPD are shown in Fig. 1. The epi-layers for SSC-WGPD were grown by a metal-organic chemical vapor deposition method. The epitaxial structure used in this study was as follows. The fiber guide section consisted of three 600 nm thick InP layers and three 50 nm thick InGaAsP ($\lambda_g = 1.24\mu m$) layers, which were grown in turn on the semi-insulated InP substrate. The mode-diameter of the fiber guide section was designed to be about 3 μm for high coupling efficiency with optical fiber. A N^+-doped 500-nm-thick InGaAsP SSC layer was grown on top of the fiber guide section, which was followed by an undoped 500 nm thick InGaAs absorption layer, 400 nm thick P-doped InP clad layer, and 100 nm thick P^+-InGaAs contact layer. As the initial process step, the ridge-typed absorption layer was defined via pattern transferring. Both dry and wet etching techniques were then used to realize the pattern, and phosphoric acid was applied to the selective wet etching as an etchant. A tapered shape SSC section was then formed using pattern transferring and a selective wet-etching process. This layer plays the major role of changing the mode size as well as the role of an n-type contact layer. After the SSC section was completed, a fiber guide section was formed. Polyimide was used to passivate the exposed surface of the P-N junction in the air, and a curing process was performed at 365°C for 1 hr, which was followed by Si_xN thin film deposition for protecting the polyimide layer from absorbing water vapor in the air. Next, P-type and N-type electrodes were deposited using a Ti/Pt/Au alloy at 400°C for 30 s, and a Au/Ge/Ni/Au alloy at 380°C for 30 s, respectively. A ground-signal-ground (GSG) coplanar typed electrode was deposited followed by a sintering process at 380°C for 30 s. Finally, a TiO_2/SiO_2 layer was deposited as an anti-reflection coating layer after the cleaving process [4].

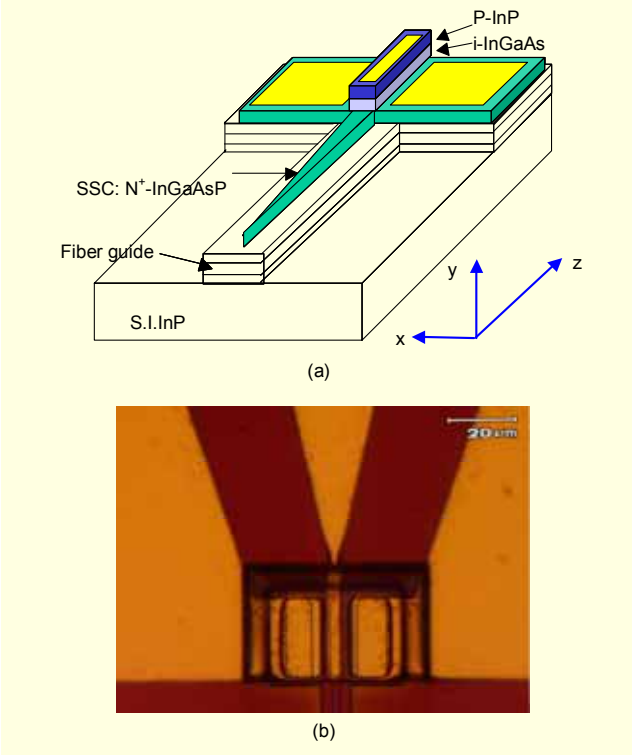

Fig. 1. A schematic diagram and microscopic image of an SSC-WGPD.

III. BPM Simulation for SSC-WGPD

A three-dimensional beam propagation method (BPM) was used to optimize the SSC-WGPDs. Figure 2 shows the BPM simulation results for SSC-WGPDs, where y and z are directions indicated in Fig. 1(a). Light from a fiber guide is transferred via a tapered SSC into the absorption region. The parameters that were considered in designing the SSC-WGPD structure are as follows. For high optical coupling efficiency with the optical fiber, the spot size of the waveguide mode on the fiber guide's side was well coincident with the spot size of the optical fiber in a circular shape. The subsequent region served to convert a relatively large spot size adiabatically into a small one without a radiation loss of light. A long (around 500 μm) laterally tapered SSC with the widths of less than 1μm and 3 μm at the start and stop portions, respectively, was selected to maximize the power transferred to the SSC section, minimize the radiation loss occurring during the spot-size-conversion process, and achieve the polarization insensitive operation. The spot-size converted light was absorbed into the absorption layer through an evanescent coupling of the modes.

Based on this BPM simulation, we found that the core process was the formation of a tapered SSC. As shown in Fig. 3,

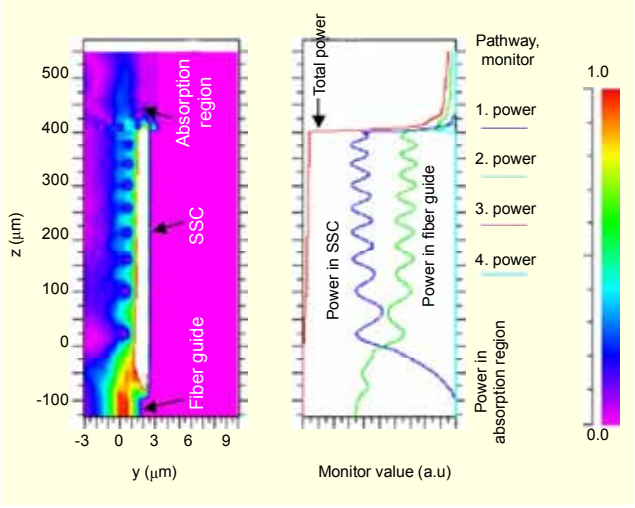

Fig. 2. BPM simulation results for SSC-WGPD.

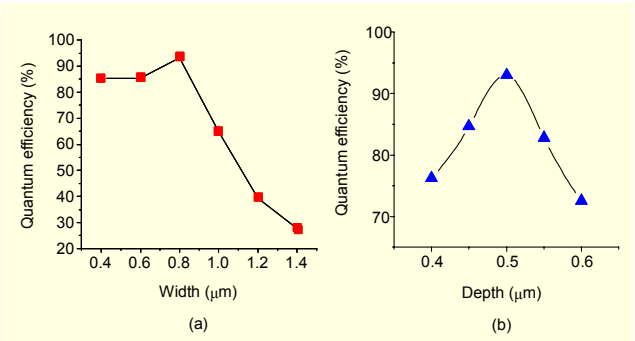

Fig. 3. The absorption quantum efficiencies as a function of the (a) width and (b) depth of start portions of a tapered SSC layer.

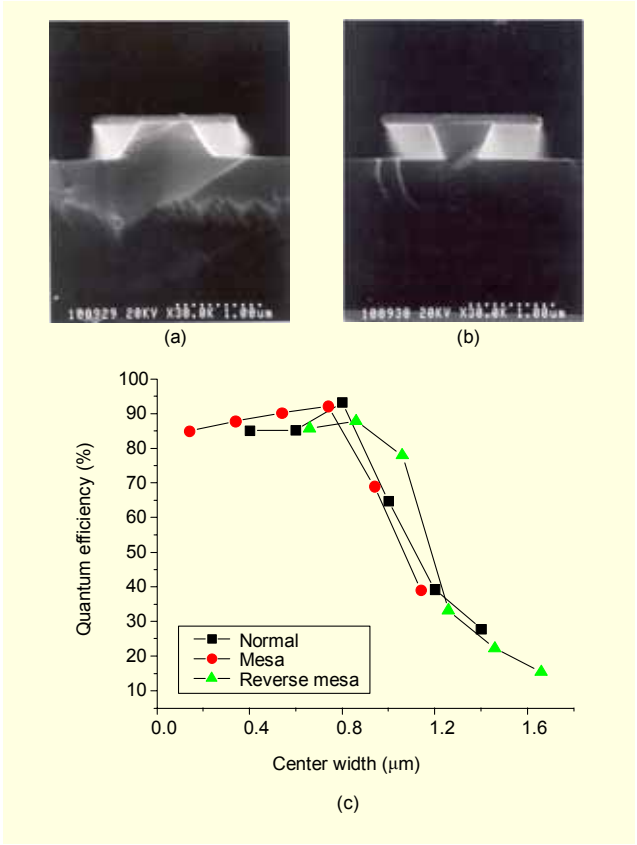

Fig. 4. Cross-sectional profiles of the SSC layer depending on stripe directions of (a) [11-0] and (b) [110], and (c) the absorption quantum efficiencies depending on the cross-sectional profiles.

if the widths of the start portions were extended to 1.0 and 1.2 μm, the absorption quantum efficiencies were lowered to 65 and 40%, respectively, in the case of a device having an absorption layer of 4 μm in width and 30 μm in length. At this time, we assumed that the coupling efficiency of light between the optical fiber and the fiber guide was 100%. However, considering the coupling loss, the practical value would be lower than the calculated value. In addition, we noted that the absorption quantum efficiencies against thickness tolerances were dropped to approximately 85% in the case of ±0.05 μm and approximately 75% in the case of ±0.1 μm. Accordingly, in order to overcome those process difficulties, which might be shared in the published reports [5]-[7], we suggested a method of exactly controlling the width and thickness of a tapered SSC by means of a selective wet-etching process and its compatible device structures. An advantage of this structure was that a waveguide pattern requiring fine control of below 1 μm, which was difficult to reproducibly attain in conventional lithography, can be easily formed using a pattern having a width in the range of 1.5 μm to 2 μm formed in a Si_xN film as shown in Figs. 4 (a) and 4(b). At this time, the undercut etching rate was approximately 0.1 μm/min with the use of phosphoric acid (H_3PO_4 : H_2O_2 = 5 : 1, RT). In addition, the thickness was controlled exactly due to wet-etch selectivity between the InP fiber guide top layer and InGaAsP SSC layer. The cross-sectional profiles of the InGaAsP SSC layer in Figs. 4 (a) and 4(b) showed mesa and reverse mesa patterns depending on the stripe directions. We noted that the absorption quantum efficiencies were the function of the center width of the start portions without regard to the cross-sectional profiles. In this study, we selected [11-0] stripe directions, so we had the mesa-type cross-sectional profiles.

IV. Characteristics of SSC-WGPD

For optimizing the coupling efficiency between the SSC-WGPD and single mode fiber, we used an aspherical lens with a superior aberration compensation feature. The simulation results in Fig. 5 are based on the Alps AC type lens and showed a nearly perfect coupling of 94%. With the use of 1.8 mm of

L1 length, the maximum responsivity was measured to be approximately 0.8 A/W, which is comparable to the highest values reported for 40 Gb/s WGPDs [5]-[7]. The 1 dB alignment tolerances reached 1.6 and 1.9 μm for vertical and horizontal directions, respectively. In addition, the fabricated SSC-WGPD showed less than 0.2 dB polarization and input light wavelength (from 1530 to 1565 nm) dependences. The discrepancies between simulated and measured coupling efficiencies could include reflection from the surface, scattering losses when propagating, and so on.

A GSG coplanar electrode was employed for on-chip probing. For high-speed measurement over approximately 40 GHz, we employed two methods for accuracy [4]. One method uses an optical heterodyne source of OMS-2010 from Lightwave, Inc., to generate modulated optical input, and the other uses an Anritsu 87300C 65 GHz vector network analyzer

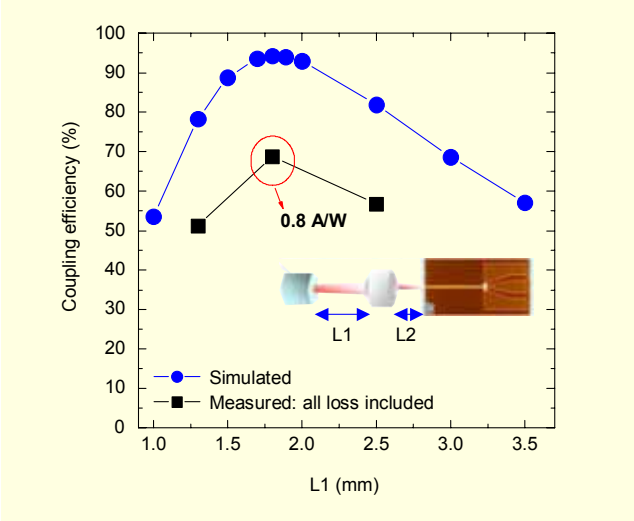

Fig. 5. The coupling efficiencies between an SSC-WGPD and single mode fibers with the use of an aspherical lens.

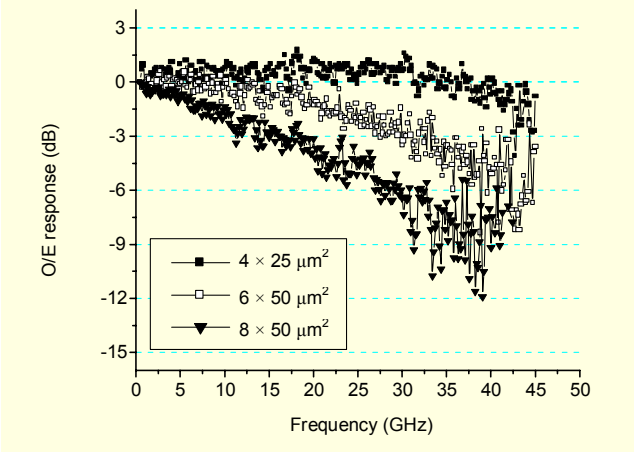

Fig. 6. SSC-WGPD optical-to-electrical response as a function of frequency.

and a calibrated transmitter. For a calibrated transmitter, a 40 Gbps electro-optic modulator from EOspace, Inc., was adopted. The small-signal 3dB bandwidth was measured to be above 40 GHz for 100 μm^2 area device and was reduced to around 20 GHz when the photodiode area was increased to 600 μm^2 as shown in Fig. 6. Figure 7 shows the value of measured 3dB bandwidth as a function of device areas. We fitted 3dB bandwidth data using

$$1/f^2 = 1/f_t^2 + 1/f_{RC}^2, \quad (1)$$

where f_t is the transit-time-limited bandwidth, and f_{RC} is RC-time-limited bandwidth assuming a 50 Ω load [10].

We found that the 20 fF parasitic capacitance value was well-fitted to our data. The 20 fF parasitic capacitance value present in the SSC-WGPD used in this study has been confirmed again through capacitance measurements as a function of device areas.

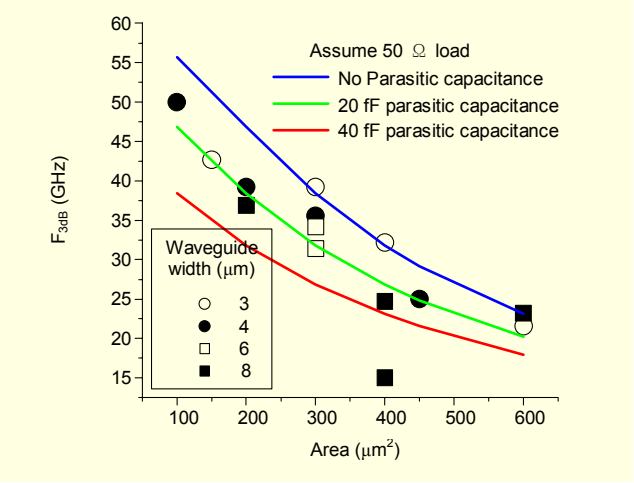

Fig. 7. The 3 dB bandwidths as a function of device areas.

V. Fabrication of PIN-TIA Front-End Optical Receivers and Their 40 Gb/s NRZ Eye Measurements

We fabricated TIA-integrated SSC-WGPD modules as shown in Fig. 8, which consisted of SSC-WGPD chips, TIA electrical pre-amplifier chips, DC bias circuits for both the PD and TIA, and electrical connections. A module housing was made of Kovar and was designed using HFSS to keep the reflection coefficient S11 below -10 dB at up to 40 GHz, which was verified through S-parameter measurements. A Wiltron V-connector was used as a microwave output part of the module. The front-end receiver module consisted of two main parts: optical and electrical assemblies. The optical assembly consisted of a single mode fiber, an aspherical lens, and a spacer with the length of 1.8 mm (L1) as shown in Fig. 5; it was aligned

to the SSC-WGPD chips and fixed to the module housing by a laser welding process. The electrical assembly was composed of a ceramic submount with a GSG coplanar transmission line and DC bias circuits for the SSC-WGPD and TIAs. Two types of commercial TIAs from Inphi, Inc., were adopted in this study. One has higher gain and the other has broader bandwidth [8]. We followed the recommended DC bias circuit designs of the TIAs with a photodiode [9]. Special attention was paid to keep all ground and bias lines below 100 μm in order to avoid any possible parasitic-related resonances. The electrical connection line between the SSC-WGPD anode and TIA input was also kept below approximately 300 μm to satisfy the required external bond wire inductance value of around 300 pH. The 1 mil Au wire with an inductance value of approximately 0.9 nH/mm was used for electrical connections [11].

A 15 mil thick ceramic submount with a GSG coplanar transmission line was fabricated as shown in Fig. 9 (a) and was shared for both TIAs. An output signal from one side among two TIA output pads were connected to the input bias line (in this case, +3.3 V) by way of a 50 ohm thin film resistor for converting differential outputs from TIAs to a single-ended one. The design of the GSG coplanar line between the TIA output and V-connector was a tapered CPW transmission line with 50 ohm characteristic impedance. The wide section of the tapered CPW was connected to the V-connector and its narrow section was bonded by the Au wire bond. The narrow section was preferred in the high frequency performance because of weak leakage coupling and radiation [12]. Vias were designed to connect top grounds to the back metallization of the submount to suppress unwanted parallel plate modes and stabilize the coplanar quasi-TEM mode. The exact dimension and position of vias were determined with HFSS simulation to achieve a low electrical return loss and insertion loss over the wide range of frequency as shown in Fig. 9(b). The initial 3 dB drop in S21 was caused due to the differential to single-ended conversion, and thus the transimpedance gain of the single-ended module was half that of the differential ones. The sharp dip in S21 and steep increase in S22 at approximately 49 GHz was originated from the cavity resonances in the submount.

The optical-to-electrical (O/E) response characteristics and 40 Gb/s NRZ eye measurement results with 0 dBm optical input power for high-gain and broad-bandwidth modules are shown in Figs. 10(a) and 10(b), respectively. A 2^{31}-1 pseudo-random bit sequence (PRBS) NRZ optical input signal at 40 Gb/s with 0 dBm input power was generated using a distributed feedback laser diode, a $LiNbO_3$ modulator, and a modulator driver with 5.5 V_{p-p} output voltage, which was driven by a 4:1 MUX from four channels of uncorrelated 10 Gb/s PRBS data. The 3 dB bandwidths of these modules were measured to be approximately 32 and 42 GHz, respectively, which was enough for delivering 40 Gb/s data streams. However, a rather steep decrease in O/E response was observed at approximately 43 GHz for a broad-bandwidth module, which could be attributed to the cavity resonance effects as shown in Fig. 9(b). The difference in resonance frequency might be originated from the virtually longer cavity, which was formed with the submount together with TIA output pads and electrical connection lines not included in the

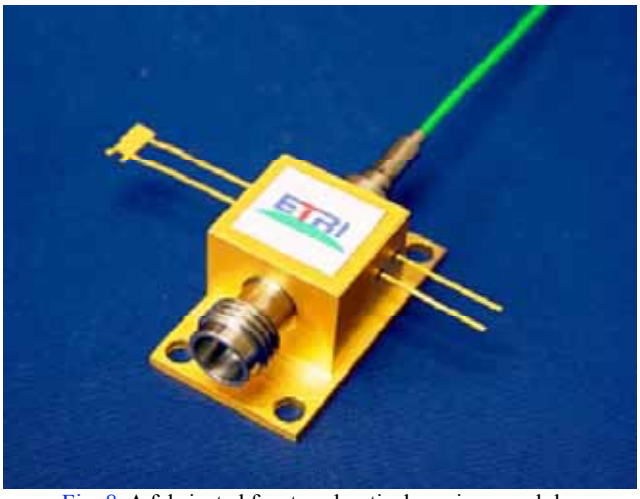

Fig. 8. A fabricated front-end optical receiver module.

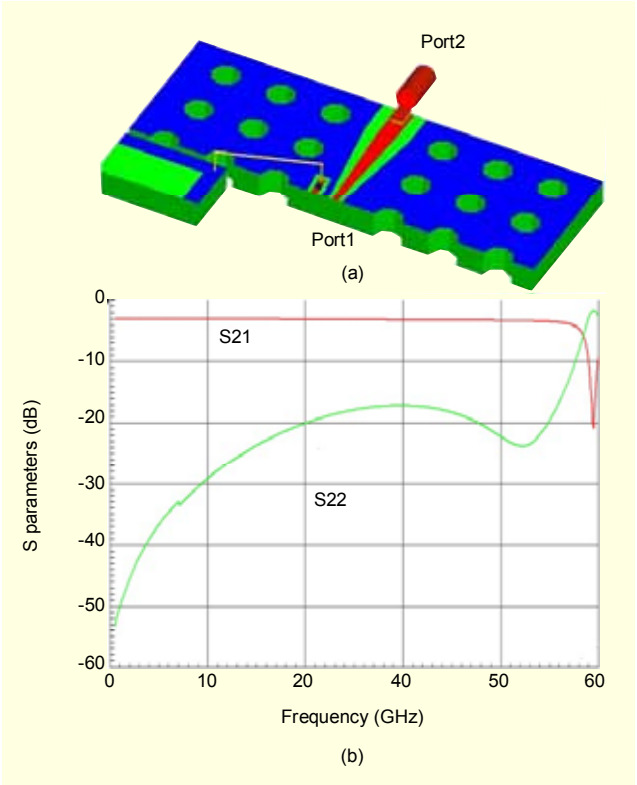

Fig. 9. (a) Schematic drawings and (b) HFSS simulation results of S parameters of a ceramic submount.

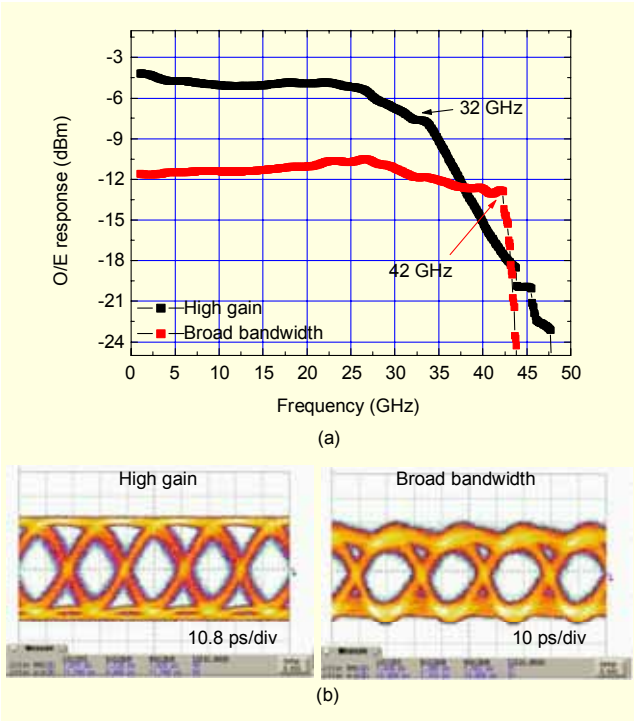

Fig. 10. (a) O/E frequency response and (b) 40 Gb/s NRZ eye diagrams of high-gain and broad-bandwidth front-end optical receivers with 0 dBm optical input power.

simulation, as shown in Fig. 9(a). This resonance effect was not clearly observed for the high-gain module, since the O/E response was already approximately 14 dB lower than that of the low frequency response.

The 40 Gb/s NRZ eye diagrams showed very clear eyes with negligible rms jitters of < 1.8 and 1.4 ps. Considering the 0.8 A/W responsivity of SSC-WGPD chips and the 15 and 35 pA/√Hz input equivalent current noise densities of high-gain and broad-bandwidth TIA chips [8], the calculated sensitivity values will be as low as -15 dBm and -11 dBm at a 10^{-10} BER, respectively [2].

VI. Conclusion

We successfully fabricated 40 Gb/s PIN-TIA front-end optical receivers using the SSC-WGPDs developed in this study. We employed a laterally tapered SSC scheme and realized the exact width and depth of a tapered SSC by a selective wet-etching process. The fabricated SSC-WGPD chips showed a high responsivity of approximately 0.8 A/W and a 3 dB bandwidth of approximately 40 GHz. The high-gain module showed its perfect relevance to high sensitivity 40 Gb/s broadband optical communications. The broad-bandwidth module will be more adequate for bandwidth-demanding applications such as 40 Gb/s RZ and 43 Gb/s optical transport network standards.

References

[1] *MCI Claims ULH Speed Record*, www.lightreading.com, Light Reading, Inc., New York, June 15, 2004.

[2] A. K. Dutta, M. Takechi, R. S. Virk, M. Kobayashi, K. Araki, K. Sato, M. Gentrup, and R. Ragle, "40 Gb/s Postamplifier and Pin/Preamplifier Modules for Next Generation Optical Front-End Systems," *IEEE J. Lightwave Tech.*, 20, 2002, pp. 2229-2238.

[3] K. Kato, "Ultrawide-Bandwidth/High-Frequency Photodetectors," *IEEE Trans. Microwave Theory and Techniques*, 47, 1999, pp. 1265-1281.

[4] J. S. Choe, Y. H. Kwon, K. S. Kim, Jeha Kim, S. C. Kong, and Y. W. Choi, "Traveling-Wave Photodetector with Asymmetrically Heterostructured Intrinsic Region," *Japanese J. Appl. Phys.* 43, 2004, pp. 5105-5109.

[5] F. Xia, J. K. Thomson, M. R. Gokhale, P. V. Studenkov, J. Wei, W. Lin, and S. R. Forrest, "An Asymmetric Twin-Waveguide High-Bandwidth Photodiode Using a Lateral Taper Coupler," *IEEE Photon. Tech. Lett.*, 13, 2001, pp. 845-847.

[6] S. Demiguel, L. Giraudet, P. P. Rossiaux, E. Boucherez, C. Jany, L. Carpentier, V. Coupe, S. F. Yee, J. Decobert, and F. Devaux, "Low-Cost, Polarization Independent Tapered Photodiodes with Bandwidth over 50 GHz," *IEE Electron.Lett.*, 37, 2001, pp. 516-518.

[7] N. Yasuoka, M. Makiuchi, M. Miyata, O. Aoki, M. Ekawa, N. Okazaki, M. Takechi, H. Kuwatsuka, and H. Soda, "High-Efficiency Pin Photo-Diodes with a Spot-Size Converter for 40 Gb/s Transmission Systems," *Proc. IOOC-ECOC* `01, 2001, pp 558-559.

[8] Datasheets of 4331TA and 4335TA, www.inphi-corp.com., 4331TA and 4335TA have 3 dB bandwidths of 38 and 50 GHz, and differential gains of 2 kΩ and 460 Ω, respectively.

[9] Application Notes of 4331TA_AN_Ver1.0.doc and 4335TA_AN_Ver1.1.doc from Inphi, Inc.

[10] G. Lucovsky, R. F. Schwarz, and R. B. Emmons, "Transit-Time Considerations in P-I-N Diodes," *J. Appl. Phys.*, 35, 1964, pp. 622-628.

[11] S. L. March, "Simple Equations Characterize Bond Wires," *Microwave & RF*, Nov. 1991, pp. 107-109.

[12] K. S. Choi, J. H. Lee, J. Lim, Y. S. Kang, Y. D. Chung, J. T. Moon, and Jeha Kim, "Optimization of Packaging Design of TWEAM Module for Digital and Analog Applications," *ETRI J.*, 26, 2004, pp.589-596.

Yong-Hwan Kwon received the BS degree in physics in 1993 and the MS and PhD degrees in semiconductor physics in 1995 and 1998, all from Seoul National University, Seoul, Korea. His thesis research was on metal-organic vapor phase epitaxy growth and the characterization of InP/InGaP self-assembled quantum dots. From 1998 to 2000, he was a research associate at the center for laser and photonics research, Oklahoma State University, where he was active in the field of GaN blue light emitting diodes. He is currently a Senior Researcher in the Basic Research Lab at Electronics and Telecommunication Research Institute (ETRI). His research interests include the design and fabrication of high-speed optoelectronic devices such as SAGCM InP/InGaAs avalanche photodetectors, high-power high-speed waveguide photodetectors, and distributed-feed-back laser integrated electroabsorption modulators.

Joong-Seon Choe was born in Seoul, Korea, on October 13, 1971. He received the BS, MS, and PhD degrees in physics from Seoul National University in 1994, 1996, and 2001. He has worked on GaAs/AlGaAs growth by MOCVD, the properties of wet-oxidized high Al content AlGaAs, and 980 nm InGaAs/GaAs quantum well laser diodes. From 2001, he has been a Senior Researcher with ETRI, where he has conducted research on high speed photodetectors for optical communication applications.

Jeha Kim received the BS and MS degrees in physics from Sogang University, Seoul, South Korea in 1982 and 1985, and the PhD degree in physics from University of Arizona, Tucson Arizona, USA in 1993. He joined ETRI in 1993, where he worked at the optoelectronics section in the development of a 10 Gbit/s laser diode for optical telecommunication. During 1995 to 1998, he worked on high temperature superconducting (HTS) passive and active microwave devices for high performance wireless communication. Since 1999, he has been working on high speed modulators and laser diodes of > 40 Gbit/s and on narrowband RF/optic conversion devices for analog communication. He is now a project leader on 60 GHz analog optical modulators and transceiver modules for RF/optic conversion. His current research interests are in the development of functional optoelectronic components, a subsystem for broadband digital and analog fiber-optic communications, and a radio-over-fiber (ROF) wireless link.

Kisoo Kim received the BS in physics in 1995 and the MS and PhD degrees in semiconductor physics in 1997 and 2000, each from Chonbuk National University, Korea. He is currently a Senior Research Engineer in the Basic Research Lab at ETRI. His current interests include the design and MOCVD growth of III-V compound semiconductors for opto-electronic devices. He is a member of Materials Research Society (MRS).

Kwang-Seong Choi received the BS degree in material science and engineering from Hanyang University, Korea, in 1993, and the MS degree in electronic material science from Korea Advanced Institute of Science and Technology, Daejeon, in 1995. From 1995 to 2001, he developed lead frame type CSPs, BLP packages, and stack packages, improving their solder joint reliability, and designed high-speed electronic packages for DDR, Rambus, and RF devices for Hynix Semiconductor. He has been a Senior Research Engineer at ETRI since 2001, where he has been designing high-speed photonic modules over 40 GHz with electrical simulation and measurement. Currently, his research area includes the development of system-on-packaging (SOP) modules for millimeter wave radio-over-fiber (ROF) links.

Byung-Seok Choi was born in Seoul, Korea, on January 16, 1973. He received the BE and ME degrees in materials science and engineering from Seoul National University, Seoul, Korea, in 1996 and 1998. In 1999, he joined the PCB R&D center, Samsung ElectroMechanics Ltd., Daejeon, Korea, where he has been engaged in research and development of high density BGA. Since October 2001, he has been with ETRI, where he has been involved in research and development of optoelectronic devices, including packaging and reliability of devices.

HoGyeong Yun received the BS degree in 1998 followed by the MS degree in 2000, both in materials science and engineering from the University of Korea. He is a Senior Member of the Engineering Staff in the Integrate Optical Module Team at ETRI.